JACS
JOURNAL OF THE AMERICAN CHEMICAL SOCIETY

ARTICLE

pubs.acs.org/JACS

Synthesis and Electron Holography Studies of Single Crystalline Nanostructures of Clathrate-II Phases K_xGe_{136} and Na_xSi_{136}

Paul Simon,*[,†] Zhongjia Tang,[‡] Wilder Carrillo-Cabrera,[†] Katherine Chiong,[‡] Bodo Böhme,[†] Michael Baitinger,[†] Hannes Lichte,[§] Yuri Grin,[†] and Arnold M. Guloy*[,‡]

[†]Max-Planck-Institut für Chemische Physik fester Stoffe, Nöthnitzer Strasse 40, 01187 Dresden, Germany

[‡]Department of Chemistry and the Texas Center for Superconductivity, University of Houston, Houston, Texas 77204-5003, United States

[§]Institute of Structure Physics, Triebenberg Laboratory for High-Resolution Electron Microscopy and Holography, Technical University of Dresden, Zum Triebenberg 50, 01328 Dresden Zaschendorf, Germany

ABSTRACT: Crystalline nanosized particles of clathrate-II phases K_xGe_{136} and Na_xSi_{136} were obtained from a dispersion of alkali metal tetrelides in ionic liquids based on DTAC/$AlCl_3$, which were slowly heated to 120−180 °C. The nanoparticles are bullet-shaped with typical dimensions of about 40 nm in width and 140−200 nm in length. Detailed structure investigations using high-resolution transmission electron microscopy (HRTEM) and electron holography reveal the crystallinity and dense morphology of the clathrate nanorods.

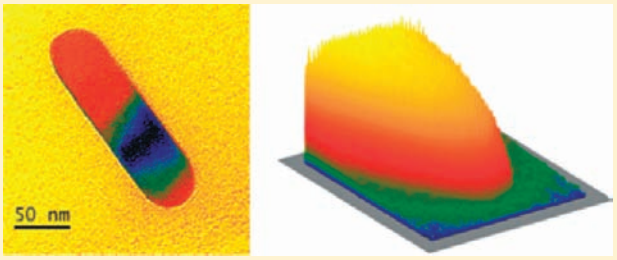

INTRODUCTION

The oxidation of reactive intermetallic phases in ionic liquids (IL) has provided new low-temperature routes to intermetallic clathrates that are usually prepared at elevated temperatures from the elements or by thermal decomposition of precursor phases. This was demonstrated by the synthesis of new metastable clathrate-II phases, the germanium allotrope Ge(*cF*136)[1] and $K_{8.6}Ge_{136}$.[2] Challenges associated with synthesizing semiconductors and intermetallic compounds with open-framework structure continue to be of major importance. In the abundant type-I and type-II clathrates,[3−5] three-dimensional arrays of tetrahedrally bonded Si, Ge, or Sn atoms form cavities, which are able to accommodate "guest" atoms. This aspect largely determines the physical properties of these compounds addressing thermoelectricity,[6−8] superconductivity,[9] and magnetism.[10]

The synthesis of nanocrystalline clathrate Si and Ge allotropes is motivated by their predicted wide optical band gaps in the same magnitude as in quantum dots and porous Si, making them promising materials in Si-based optoelectronic devices.[11] In addition, theoretical studies have predicted enhanced optoelectronic properties of nanostructured clathrate materials.[12−15] Much of the research on the synthesis of nanostructured semiconductors has been focused on direct band gap semiconductors such as the III−V and II−VI families. Success in these two classes of semiconductors has been to a large extent due to the ability to grow colloidal populations of nanocrystals using solution techniques.[16] Similar synthesis techniques that allow for the preparation of controlled nanoscale sizes and shapes of intermetallic clathrate particles have not yet been reported.

However, the preparation of an entirely X-ray amorphous bulk product consisting of potassium (∼8 at. %) and germanium (∼92 at. %) was reported from the oxidation of K_4Ge_9 by an IL based on *n*-dodecyltrimethylammonium chloride (DTAC) and $AlCl_3$. By annealing at 370 °C, the X-ray amorphous product was transformed to crystalline clathrate-II $K_{8.6}Ge_{136}$.[2] The X-ray amorphous oxidation product might thus feature crystalline clathrate domains below the coherence length of X-ray radiation.

Herein, we report on a HRTEM and electron holography study on clathrate-II nanoparticles obtained from reactions of alkali metal silicides and germanides dispersed in a mixture of crown ether and DTAC/$AlCl_3$.

EXPERIMENTAL SECTION

Synthesis. The precursor K_4Ge_9 was prepared by heating the elements (K, Chempur 99.9%; Ge, Chempur, 4 N) to 1200 °C within sealed Ta tubes using an induction furnace, and then annealing for 8 h in a tube furnace at 600 °C. X-ray powder diffraction (XRPD) patterns showed a single phase K_4Ge_9.[17,18] The precursor with the nominal composition $NaSi_{2.25}$ was prepared by inductive heating of the stoichiometric mixture of the elements at 1200 °C for 10 min, followed by annealing at 800 °C for an hour. XRPD patterns of the as-prepared $NaSi_{2.25}$ indicated a mixture of Na_4Si_4 and α-Si. The IL was prepared by mixing dodecyltrimethylammonium chloride (DTAC, Merck) and $AlCl_3$ (Merck) in a molar ratio 1:1 under argon atmosphere. The precursors, K_4Ge_9 (60 mg) or $NaSi_{2.25}$ (50 mg), were mixed with 20 mg of 18-crown-6 (Merck, for synthesis) and added to 1 g of IL. The mixtures were heated over 5 h to 120−180 °C, and were kept for 3 days at this temperature in closed Duran vessels under argon atmosphere. The resulting product was treated as follows: the mixture was first washed with

Received: March 9, 2011
Published: April 22, 2011

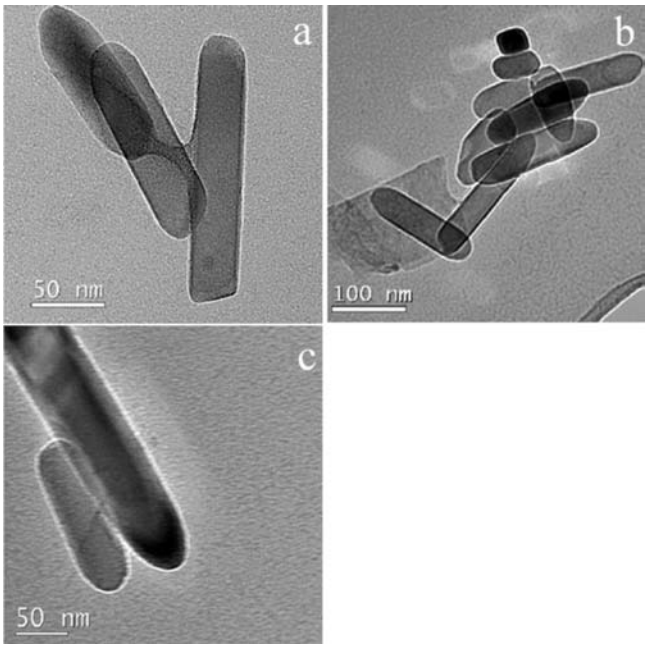

Figure 1. (a–c) Rod-shaped nanoparticles of K_xGe_{136}.

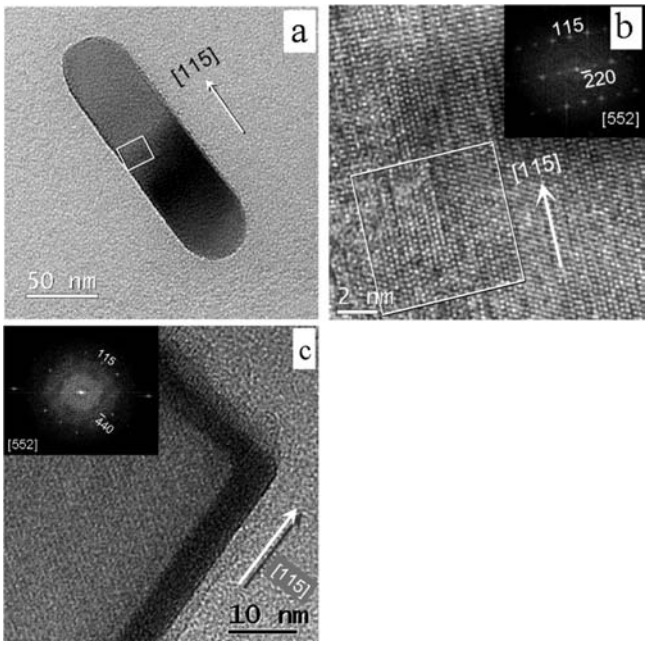

Figure 2. (a) A rod-shaped nanoparticle of the clathrate-II K_xGe_{136} with the main axis parallel to [115]. (b) Enlarged HRTEM image of the region marked in (a) with view along [55$\bar{2}$] direction (FFT image inserted). (c) HRTEM image of a rod-shaped particle of Na_xSi_{136} with corresponding FFT image.

acetone (5 mL), centrifuged (4000 rpm, 2585*g* for 10 min), and the yellow acetone extract was separated. The dark gray residue was further washed with ethanol (5 mL), centrifuged (for 10 min), and separated. The isolated solid was then suspended in absolute ethanol and taken for TEM studies.

The initial oxidation products of K_4Ge_9 appeared X-ray amorphous, based on very broad "humps" in their XRD powder patterns. Subsequent

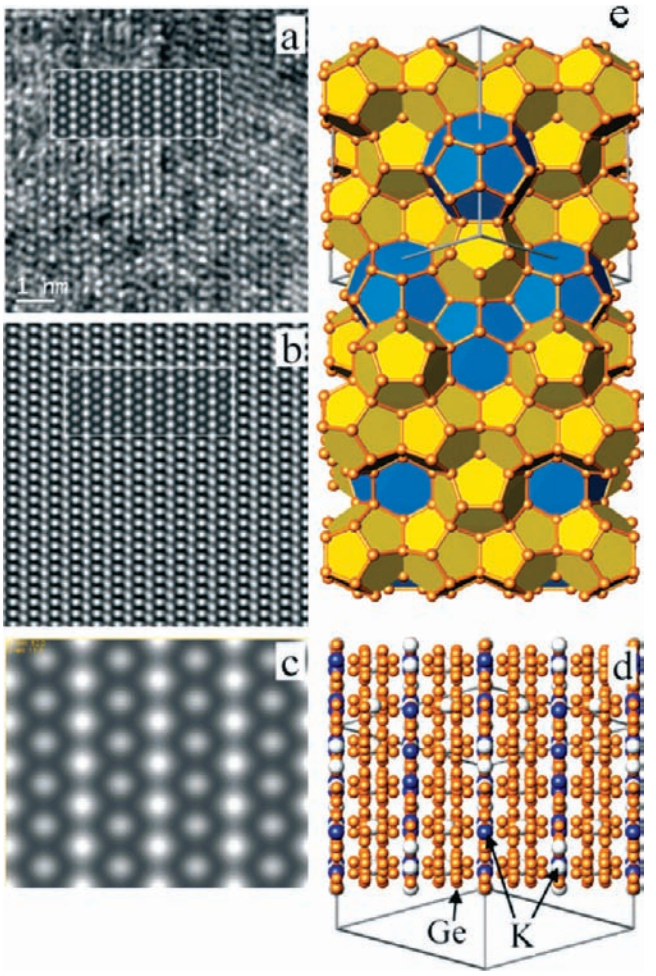

Figure 3. (a) HRTEM image of the clathrate-II K_xGe_{136} in [55$\bar{2}$] direction taken from the marked region in Figure 2b (inset: simulated image for composition K_8Ge_{136}, defocus = −52 nm, thickness = 12 nm). The lattice appears locally distorted due to local tilting and overlap with amorphous carbon substrate. (b) Filtered and averaged image of (a). (c) The simulated image in comparison with the crystal structure (d). Ge atoms are displayed in yellow, K atoms (site 8*b*) in blue, and the empty site 16*c* in white. (e) Packing of the polyhedra in the clathrate-II structure with hexacaidecahera occupied by K (blue) and empty dodecahedra (yellow).

investigations, using HRTEM and electron holography, indicated the products to be crystalline clathrate nanoparticles. Thermal treatment of the nanoparticles at 370 °C for 2 days resulted in the formation of polycrystalline clathrate-II phase. This result compares to the formation of polycrystalline $K_{8.6}Ge_{136}$, from an X-ray amorphous product obtained by reaction of K_4Ge_9 with DTAC/$AlCl_3$.[2] Long-term exposure of the clathrate-II nanoparticles to air revealed the material to be stable to oxidation.

Similar studies were performed on the products of the oxidation of $NaSi_{2.25}$, resulting in nanocrystalline particles of a clathrate-II phase. The addition of 18-crown-6 was found to influence the distinct shape of the clathrate nanoparticles.

High-Resolution Transmission Electron Microscopy. Studies were performed on the washed products suspended in ethanol. For electron microscopy, a drop of the ethanol suspension was placed onto the electron microscopy grid (SPI Supplies, West Chester, PA). After 1 min, the excess was removed by a blotting paper, and thereafter the microscopy grids were air-dried. For further experiments, the grids were

dx.doi.org/10.1021/ja201728v |*J. Am. Chem. Soc.* 2011, 133, 7596–7601

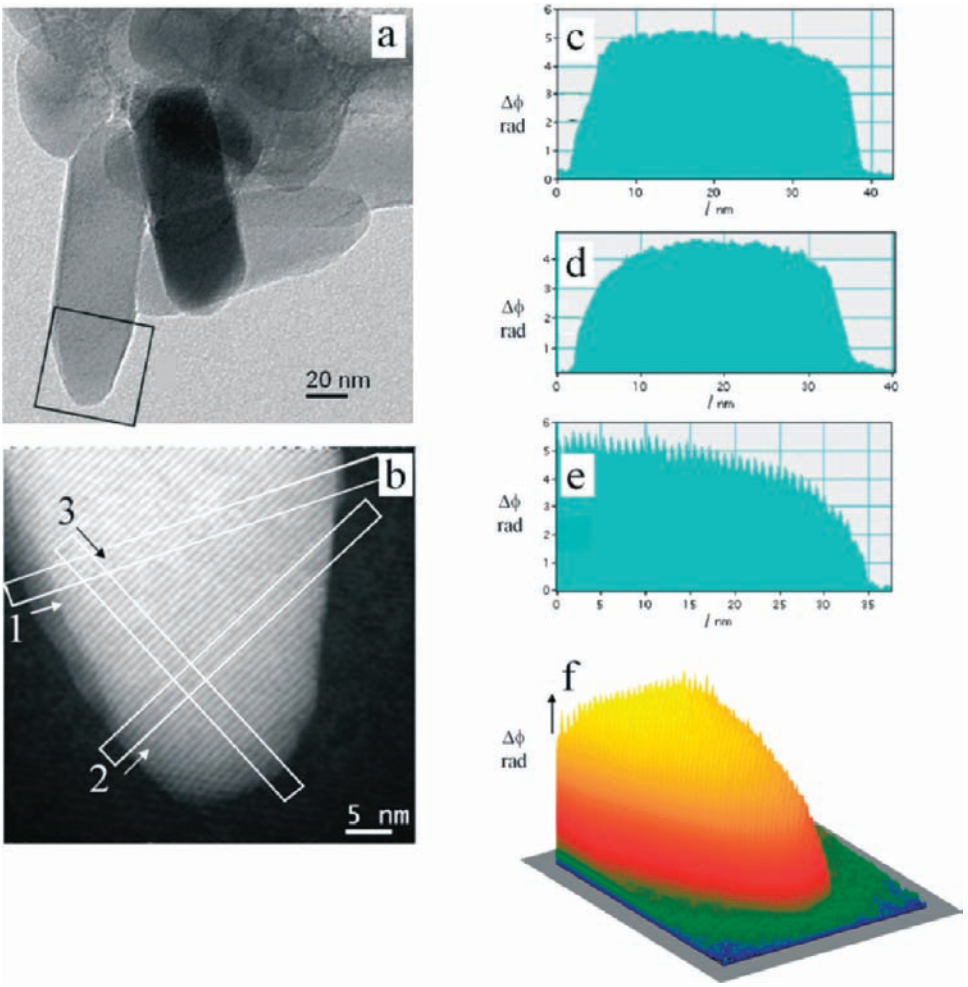

Figure 4. (a) Overview HRTEM image K_xGe_{136} nanorods. (b) Reconstructed high-resolution phase image of the electron hologram recorded from the region marked in (a). Phase profiles of (c) region 1, (d) region 2, and (e) region 3, demonstrating that the sample is not hollow. The phase shift $\Delta\phi$ readout from the phase profiles corresponds to a maximum particle thickness of 48 nm. In the phase profile (e), the (111) lattice planes of clathrate-II are clearly observed. (f) The topography of the nanoparticle tip generated from the phase image in (b) shows steep walls and a flat top.

covered with a holey carbon film. Conventional transmission electron microscopy was performed using a Philips CM200 FEG\ST Lorentz electron microscope at an acceleration voltage of 200 kV.

Electron Holography. To understand the detailed features of the clathrate nanoparticles, off-axis electron holography was performed. Use of electron holography overcomes the problems associated with the analysis of detailed object structures that give rise to a phase modulation of the object exit wave.[19,20] Examples of these problems are electrical and magnetic fields,[21−24] as well as the determination of slight differences of thickness, chemical composition, or density.[25,26] As electron holography records both the amplitude and the phase of the object's exit wave in focus, it allows the quantitative reconstruction of both the amplitude image and the phase image. Off-axis holograms are produced by means of an electrostatic biprism inserted into the electron microscope in front of the intermediate image as beam splitter. The biprism, built of a positively charged wire, superimposes a plane reference wave running through a vacuum to the object's exit wave, giving rise to an interference pattern in the image plane.[19,20] The hologram was recorded by means of a CCD camera and transferred to a computer where the phase information is retrieved by numerical analysis (Digital Micrograph software, Gatan Inc., U.S.). Analysis of the phase profile of the investigated nanoparticles in reconstructed phase images of holograms enabled us to distinguish between different morphologies and to determine whether the investigated nanocrystalline particles were compact/solid or hollow.[26,27]

RESULTS AND DISCUSSION

The solubility of cluster anions such as Pb_9^{4-}, Sn_9^{4-}, and Ge_9^{4-} in polar solvents as NH_3 or ethylenediamine has been shown by electrochemical methods[28−30] and by Raman spectroscopy.[31] Raman spectra of ethylenediamine solutions of K_4Ge_9 show characteristic bands of condensed polyanions $[Ge_9^{n-}]_x$.[32] Crystalline solids containing oxidatively coupled cluster anions of silicon and germanium have also been reported.[33−36] These results indicate a high reactivity of the naked isolated germanium cluster anions in the weakly acidic amine solvents. In an ionic liquid DTAC/$AlCl_3$, the compounds are oxidized by acidic protons of the quaternary ammonium cations *n*-DTA^+ in a heterogeneous liquid−solid reaction under formation of H_2, 1-dodecene, trimethylamine, and the metal chloride.[1] In this case, dissolving of germanium cluster anions is unlikely to be involved in the oxidation of intermetallic compounds such as K_4Ge_9.[37]

HRTEM images of the solid products obtained from the oxidation by the IL show mostly crystalline clathrate-II nanoparticles,

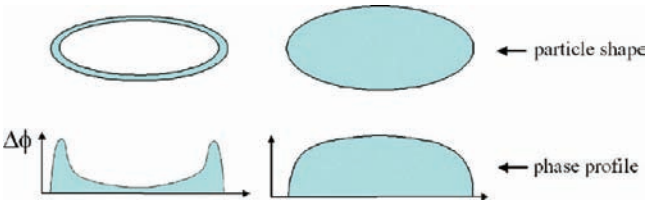

Figure 5. The phase profile and the corresponding model of a hollow nanotube in cross section (left) as compared to a phase profile and model structure of a compact nanorod (right). Electron phase images demonstrate a clear difference between hollow and solid bodies.

with a minor content of amorphous particles. Well-shaped elongated rod-like nanoparticles of K_xGe_{136} were identified with a bimodal distribution with an average length of about 191 (±26) or 135 (±16) nm and widths in the range of 43 (±7) or 41 (±5) nm, respectively (Figure 1). Fourier transforms of the HRTEM patterns reveal that the rod-shaped nanoparticles all have *d*-spacings in agreement with the cubic clathrate-II structure of $K_{8.6}Ge_{136}$ (Figures 2a,b). In our former investigation, an X-ray amorphous solid obtained under similar conditions at 300 °C had a bulk composition corresponding to $K_{12}Ge_{136}$.[2] Therefore, we assume a similarly high potassium content for the nanocrystalline clathrate particles (similar composition is expected for the sodium clathrate).

Analogous results were observed for the clathrate-II particles of Na_xSi_{136} (Figure 2c). Most of the nanoparticles were found to consist of one crystalline domain, thus being nanosingle crystals. In the HRTEM micrographs, the crystal lattice appears slightly tilted due to local distortions at certain regions. However, the agreement between experimental and simulated HRTEM images is satisfactory (Figures 3a,b). A simulated image for clathrate-II unit cell is shown in Figure 3c, with the crystal structure of K_8Ge_{136} viewed along $[55\bar{2}]$ direction in Figure 3d,e.

A notable feature of the HRTEM images of the Ge and Si clathrate nanoparticles is a rather dark outline of the walls of the nanoparticle, as compared to a lighter shaded inner structure (Figures 1 and 2). Such features can be caused by hollow structures, as it was found for a variety of hollow tubular nanostructures and spherical shells.[38−41] To determine the inner structure of the nanoparticles, high-resolution electron holograms were recorded in a selected region of the crystalline nanoparticle of the K_8Ge_{136} clathrate, which is marked by a frame in the conventional HRTEM image (Figure 4a). The reconstructed phase image of the clathrate nanoparticle is shown in Figure 4b and provides detailed information on the morphology. The experimental phase profiles (Figures 4c−e) show that the particles are compact (Figure 5) and that the rim observed in the conventional HRTEM experiment is an experimental artifact. The brick-like shape with steep walls and a flat and smooth top is demonstrated by profiles in Figure 4c−e. Remarkably, the (111) lattice planes of the clathrate-II framework are directly observed in the phase profile as a weak sinusoidal modulation at the top of the profile, having an amplitude of about 0.15 rad (Figure 4e). The maximum thickness of the brick-shaped particle amounts to about 48 nm corresponding to a phase shift $\Delta\phi$ of 5.0 rad as measured from the phase profile of Figure 4c, assuming a mean inner potential U_i of 14.3 V for K_8Ge_{136}. The phase shift is proportional to the inner potential U_i of the sample integrated along the electron trajectory, the sample thickness, and the microscope constant (0.0073 V^{-1} nm^{-1}).[26] The inner potential

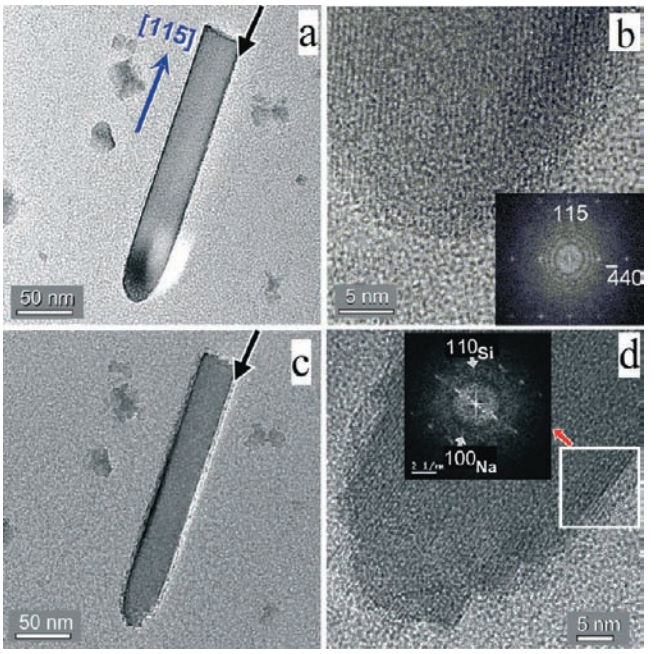

Figure 6. (a,b) Overview and HRTEM image of a nanoparticle of a clathrate-II Na_xSi_{136} elongated along [115] with corresponding FFT image. (c,d) The same particle with irradiation damage and an FFT image calculated for the marked region. After irradiation, small crystals of sodium and α-Si are segregated to the surface, which were identified by extra peaks in the FFT image.

was estimated by summing the atomic scattering factors as given by Doyle-Turner.[42,43] The error in thickness determination caused by dynamical effects is estimated to be smaller than 5%. Because the crystal is weakly diffracting and the wedge-shaped background has to be taken into account with about 5% tolerance, a total error of about 10% is expected from this procedure. Finally, a 3D representation of the brick-shaped particle tip is shown in Figure 4f, generated from the phase image of Figure 4b. This also clearly shows the smoothness of the surface of the K_xGe_{136} rod-shaped crystalline nanoparticle.

Nanoparticles of the sodium silicon clathrate, Na_xSi_{136}, obtained from the analogous oxidation reactions, show similar sizes and shapes as it was observed for the K_xGe_{136}. The overview HRTEM micrograph (Figure 6a) shows a bullet-shaped rod-like nanoparticle of Na_xSi_{136} with clathrate-II type of structure. The long axis of the single crystalline nanorod is oriented along [115] direction (see also Figures 2c and 6b). As in the K_xGe_{136} crystalline nanoparticles, the Na_xSi_{136} particles consist of only one crystalline domain. Differently from K_xGe_{136}, the Na_xSi_{136} nanoparticle gradually decomposed under electron irradiation in dynamic high vacuum (Figure 6c and d). In the overview image of Figure 6c, the growth of smaller nanoparticles on the edges of the larger clathrate nanoparticle is observed after exposure to a high dose of electrons (about 2500 electrons/$Å^2$). From peak distances in the FFT images, the nanoparticles at the surface could be identified as sodium (d_{100} = 4.3 Å) and α-silicon (d_{110} = 3.9 Å). The forbidden reflections of the sodium (a = 4.2906 Å) and silicon (a = 5.4309 Å) nanocrystals are observed due to dynamical effects and are marked with arrows in Figure 6d (inset). As the dominant reflections attributable to the clathrate-II framework are still observed (FFT in Figure 6b, inset), the segregation of Na and Si particles has no influence on the

dx.doi.org/10.1021/ja201728v | *J. Am. Chem. Soc.* 2011, 133, 7596–7601

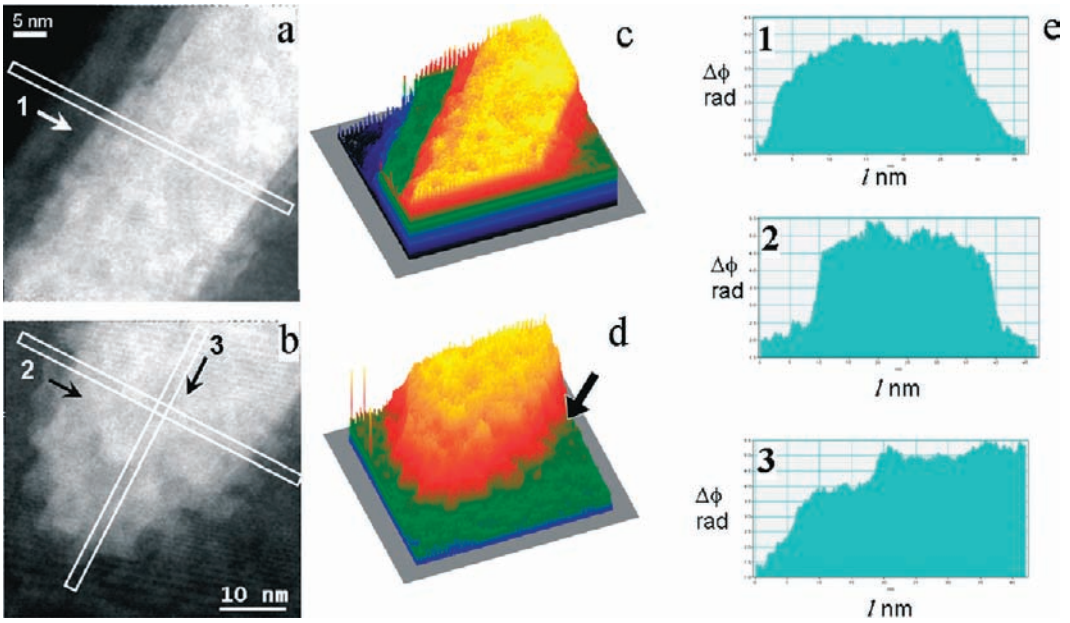

Figure 7. High-resolution electron holography study on selected regions of the nanoparticle in Figure 6 after irradiation damage: (a,b) phase images and (c,d) their corresponding 3D visualizations (phase magnitude represented by the color). (e) Phase profiles of regions 1−3 in (a) and (b), demonstrating that the sample is not hollow. Maximum estimated thickness of the brick is about 50 nm, assuming a mean inner potential of 11.85 V for Na_8Si_{136}. The nanoparticle shows a bumpy tip due to segregated Na and α-Si crystals.

crystallinity of the core structure of the clathrate-II silicon framework (in Figure 6d). During the investigation, the width of the clathrate nanoparticle shrunk from 37 to 33 nm.

High-resolution electron holograms were recorded in selected regions of the Na_xSi_{136} nanoparticle, for example, from the tip as displayed in the conventional HRTEM image in Figure 6d. The corresponding reconstructed phase images of the electron holograms are displayed in Figure 7a and b. Phase profiles of regions 1−3 of the Na_xSi_{136} clathrate rod-like nanoparticle were extracted from the reconstructed phase images (see Figure 7a and b) and are shown in Figure 7e. Analyses of the profiles unambiguously demonstrate that the clathrate-II Na_xSi_{136} nanoparticle is compact. The maximum estimated thickness of the brick is about 50 nm, assuming a mean inner potential of 11.85 V calculated for the composition Na_8Si_{136}. The 3D representation as illustrated in Figure 7c and d further reveals significant roughness of the surface of the clathrate-II nanoparticle, as compared to K_xGe_{136} (Figure 4f). The increased roughness can be largely attributed to the segregation of nanocrystalline sodium and α-silicon particles from the clathrate-II Na_xSi_{136} nanoparticle. The diameters of the Na and Si particles, of approximately 4−7 nm, were estimated from the images in Figure 7c and d and the extracted phase profiles.

CONCLUSION

The formation of single crystalline nanoparticles with clathrate-II crystal structure by oxidation of intermetallic precursor phases by an ionic liquid was demonstrated. Morphology and habitus of the nanoparticles were clearly revealed by means of electron holography and high-resolution electron microscopy. The nanocrystals of clathrate-II K_xGe_{136} and Na_xSi_{136} form elongated compact rods with bullet-like tips with about 40 nm in width and 140−200 nm in length. Although we found an elongation along [115] direction by chance for both cases, we suggest that the growing direction is in reality [001], which has a deviation of 15.8° from [115].

Following the chemistry of zeolites and aluminosilicates, new types of anionic open structures can be expected by varying the synthesis conditions (e.g., temperature, organic cations, templates and oxidizers, and anions) or by aliovalent doping. We are currently extending the new chemical route to explore whether this is a general route to novel silicon and germanium crystalline nanostructures.

AUTHOR INFORMATION

Corresponding Author
simon@cpfs.mpg.de; aguloy@uh.edu

ACKNOWLEDGMENT

B.B. and Yu.G. gratefully acknowledge funding by the European Union and the Free State of Saxony (SAB project 13853/2379), and M.B., Yu.G., and H.L. gratefully acknowledge financial support by the Deutsche Forschungsgemeinschaft (SPP 1415, "Kristalline Nichtgleichgewichtsphasen (KNG) - Präparation, Charakterisierung und in situ-Untersuchung der Bildungsmechanismen"). A.M.G., Z.T., and K.C. acknowledge support from the the NSF (CHE-0616805) and the Welch Foundation (E-1297).

REFERENCES

(1) Guloy, A. M.; Tang, Z.; Baitinger, M.; Ramlau, R.; Grin, Y. *Nature* **2006**, *443*, 320–323.
(2) Guloy, A. M.; Tang, Z.; Ramlau, R.; Böhme, B.; Baitinger, M.; Grin, Yu. *Eur. J. Inorg. Chem.* **2009**, *17*, 2455–2458.
(3) Kovnir, K. A.; Shevelkov, A. V. *Russ. Chem. Rev.* **2004**, *73*, 923–938.
(4) Beekman, M.; Nolas, G. S. *J. Mater. Chem.* **2008**, *18*, 842–851.
(5) Cros, C.; Pouchard, M. *C. R. Chim.* **2009**, *12*, 1014–1056.

(6) Nolas, G. S.; Cohn, J. L.; Slack, G. A.; Schujman, S. B. *Appl. Phys. Lett.* **1998**, *73*, 178–180.
(7) Iversen, B. B.; Palmqvist, A. E. C.; Cox, D. E.; Nolas, G. S.; Stucky, G. D.; Blake, N. P.; Metiu, H. *J. Solid State Chem.* **2000**, *149*, 455–458.
(8) Cohn, J. L.; Nolas, G. S.; Fessatidis, V.; Metcalf, T. H.; Slack, G. A. *Phys. Rev. Lett.* **1999**, *82*, 779–782.
(9) Connétable, D.; Timoshevskii, V.; Masenelli, B.; Beille, J.; Marcus, J.; Barbara, B.; Saitta, A. M.; Rignanese, G.-M.; Melinon, P.; Yamanaka, S.; Blase, X. *Phys. Rev. Lett.* **2003**, *91*, 247001:1–4.
(10) Paschen, S.; Carrillo-Cabrera, W.; Bentien, A.; Tran, V. H.; Baenitz, M.; Grin, Yu.; Steglich, F. *Phys. Rev. B* **2001**, *64*, 214404:1–11.
(11) Adams, G. B.; O'Keefe, M.; Demor, A. A.; Sankey, O. F.; Huang, J. M. *Phys. Rev. B* **1994**, *49*, 8048–8053.
(12) Moriguchi, K.; Munetoh, S.; Shintani, A. *Phys. Rev. B* **2000**, *62*, 7138–7143.
(13) Durandurdu, M. *Phys. Status Solidi B* **2006**, *243*, R7–R9.
(14) Sirichantaropass, S.; García-Suárez, V. M.; Lambert, C. J. *Phys. Rev. B* **2007**, *75*, 075328:1–5.
(15) Ponomareva, I.; Richter, E.; Andriotis, A. N.; Menon, M. *Nano Lett.* **2007**, *7*, 3424–3428.
(16) Kudera, S.; Carbone, L.; Zanella, M.; Cingolani, R.; Parak, W. J.; Manna, L. *Phys. Status Solidi A* **2006**, *203*, 1329–1336.
(17) von Schnering, H. G.; Baitinger, M.; Bolle, U.; Carrillo-Cabrera, W.; Curda, J.; Grin, Y.; Heinemann, F.; Llanos, J.; Peters, K.; Schmeding, A.; Somer, M. *Z. Anorg. Allg. Chem.* **1997**, *623*, 1037–1039.
(18) Ponou, S.; Fässler, T. F. *Z. Anorg. Allg. Chem.* **2007**, *633*, 393–397.
(19) Lichte, H.; Lehmann, M. *Rep. Prog. Phys.* **2008**, *71*, 016102: 1–46.
(20) Völkl, E., Allard, L. F., Joy, D. C., Eds. *Introduction to Electron Holography*; Kluwer Academic/Plenum Publishers: New York, 1999.
(21) McCartney, M. R.; Agarwal, N.; Chung, S.; Cullen, D. A.; Han, M.-G.; He, K.; Li, L.; Wang, H.; Zhou, L.; Smith, D. J. *Ultramicroscopy* **2010**, *110*, 375–382.
(22) den Hertog, M. I.; Schmid, H.; Cooper, D.; Rouviere, J. L.; Bjork, M. T.; Riel, H.; Rivallin, P.; Karg, S.; Riess, W. *Nano Lett.* **2009**, *9*, 3837–3843.
(23) Fujita, T.; Hayashi, Y.; Tokunaga, T.; Yamamoto, K. *Appl. Phys. Lett.* **2006**, *88*, 243118:1–3.
(24) Dunin-Borkowski, R. E.; McCartney, M. R.; Frankel, R. B.; Kardynal, B.; Smith, D. J. *Science* **1998**, *282*, 1868–1870.
(25) Simon, P.; Lichte, H.; Drechsel, J.; Formanek, P.; Graff, A.; Wahl, R.; Mertig, M.; Adhikari, R.; Michler, H. G. *Adv. Mater.* **2003**, *15*, 1475–1481.
(26) Lichte, H.; Formanek, P.; Lenk, A.; Linck, M.; Matzeck, C.; Lehmann, M.; Simon, P. *Annu. Rev. Mater. Res.* **2007**, *37*, 539–588.
(27) Allard, L. F.; Völkl, E.; Kalakkad, D. S.; Datye, A. K. *J. Mater. Sci.* **1994**, *29*, 5612–5614.
(28) Smyth, F. H. *J. Am. Chem. Soc.* **1917**, *39*, 1299–1312.
(29) Zintl, E.; Gonbeau, J.; Dullenkopf, W. *Z. Phys. Chem. A* **1931**, *154*, 1–46.
(30) Diehl, L.; Khodadadeh, K.; Kummer, D.; Strähle, J. *Chem. Ber.* **1976**, *109*, 3404–3418.
(31) Carrillo-Cabrera, W.; Cardoso Gil, R.; Somer, M.; Persil, Ö.; von Schnering, H. G. *Z. Anorg. Allg. Chem.* **2003**, *629*, 601–608.
(32) Kircali, A. Master Thesis, Koc University, Istanbul, 2007.
(33) Hauptmann, R.; Fässler, T. F. *Z. Anorg. Allg. Chem.* **2003**, *629*, 2266–2273.
(34) Downie, C.; Tang, Z.; Guloy, A. M. *Angew. Chem., Int. Ed.* **2000**, *39*, 337–340.
(35) Downie, C.; Mao, J.-G.; Parmar, H.; Guloy, A. M. *Inorg. Chem.* **2004**, *43*, 1992–1997.
(36) Ungrinov, A.; Sevov, S. *Inorg. Chem.* **2003**, *42*, 5789–5791.
(37) Böhme, B. Ph.D. Thesis, TU Dresden, Logos Verlag Berlin, 2010.
(38) Prinz, V. Y.; Seleznev, V. A.; Gutakovsky, A. K.; Chehovskiy, A. V.; Preobrazhenskii, V. V.; Putyato, M. A.; Gavrilova, T. A. *Phys. E* **2000**, *6*, 828–831.
(39) Fan, S. S.; Chapline, M. G.; Franklin, N. R.; Tombler, T. W.; Cassell, A. M.; Dai, H. J. *Science* **1999**, *283*, 512.
(40) Xia, Y. N.; Yang, P. D.; Sun, Y. G.; Wu, Y. Y.; Mayers, B.; Gates, B.; Yin, Y. D.; Kim, F.; Yan, Y. Q. *Adv. Mater.* **2003**, *15*, 353–389.
(41) Burda, C.; Chen, X. B.; Narayanan, R.; El-Sayed, M. A. *Chem. Rev.* **2005**, *105*, 1025–1102.
(42) Gajdardziska-Josifska, M.; Carim, A. H. In *Introduction to Electron Holography*; Völkl, E., Allard, L. F., Joy, D. C., Eds.; Kluwer Academic/Plenum Publishers: New York, 1999; pp 267−293.
(43) Lubk, A.; Wolf, D.; Lichte, H. *Ultramicroscopy* **2010**, *110*, 438–446.